CRACK RESISTANCE DETERMINATION FROM THE CHARPY IMPACT TEST

R. Chaouadi and J.L. Puzzolante
SCK•CEN
Boeretang 200
2400 Mol, Belgium

ABSTRACT

Many engineers and scientists investigated the possibility to correlate Charpy impact energy with the fracture toughness. As a result, many empirical correlations can be found in literature. However, most of these correlations have a limited application range due primarily to their empirical basis. Recently, a simple procedure based on the proportionality between crack length and absorbed energy was provided to determine crack length from the load-displacement test record. This procedure was validated on a large number of materials using various cracked geometries. The main objective of this paper is to investigate the possibility to apply a similar procedure to a V-notched geometry, namely the Charpy specimen. Such an evaluation would lead to estimate the material crack resistance from a single Charpy-V impact test.
By performing a number of well selected experiments, it is demonstrated that such a correlation exists and can lead to an accurate determination of both static as well as dynamic crack resistance from the simple Charpy impact test.

Introduction

The Charpy impact test is one of the most fascinating mechanical tests as one try to extract many properties than originally expected. In particular, many engineers and scientists investigated the possibility to correlate Charpy impact energy with the fracture toughness. Indeed, the Charpy impact test is considered as a cheap and easy test in comparison to the fracture toughness test which requires precracking and more sophisticated instrumentation to monitor crack extension. As a result, many empirical correlations were proposed in literature [1-8]. However, most of these correlations are limited in terms of range of application due primarily to their empirical basis. Indeed, these correlations are established on experimental data including Charpy impact energy, static fracture toughness and static yield strength, lumping therefore effects related to loading rate, notch acuity and crack length-to-width ratio. We have shown the limitation of such an empirical treatment in [9], in particular the invariability of the Charpy impact energy at upper shelf while static fracture toughness decreases with increasing temperature.
Recently, a simple procedure was provided to determine crack length from the load-displacement test record [10]. The basic underlying idea is that crack length is proportional to the square of absorbed energy. This procedure was validated on a large number of materials using various cracked geometries. It was also demonstrated to be applicable to shallow crack configurations as well as large crack extensions [10-11]. The main objective of this paper is to investigate the possibility to apply a similar procedure to a V-notched geometry, namely the Charpy V-notched specimen, to determine the quasi-static crack resistance. It was shown, in an accompanying paper [9], that there are serious indications that are supporting such a derivation. Three effects must be considered

- Effect of the notch/crack acuity: in the Charpy impact specimen, the V-notch radius is 0.25 mm, which is significantly larger than the infinitely small crack tip radius ($\rightarrow 0$);
- Effect of the notch/crack depth–to–width ratio: in the Charpy impact specimen, the notch depth–to–width ratio is 0.2 mm while it is close to 0.5 for fracture mechanics specimens;
- Effect of the loading rate: the Charpy impact test is dynamic while fracture mechanics tests are quasi-static.

In order to correctly take these effects into account, we performed a number of dedicated tests to derive the individual effects. In the following, the energy normalization procedure will be briefly recalled and additional information on how it can be applied to the instrumented Charpy impact test will be given.

Crack resistance determination procedure

The crack resistance behavior is obtained using the following procedure. The J-integral calculation is based on the ASTM E-1820 standard [12] which, for the single edge bend geometry, gives the following equation:

$$J_{(i)} = \frac{K_{(i)}^2 \left(1-\nu^2\right)}{E} + \left[J_{pl(i-1)} + \frac{\eta}{W-a_{(i-1)}} \frac{U_{(i)} - U_{(i-1)}}{B_n} \right] \left(1 - \frac{a_{(i)} - a_{(i-1)}}{W - a_{(i-1)}} \right) \tag{1}$$

where U is the area under the load-displacement curve, W, B, B_n and a_0 are the specimen width, thickness, net thickness and crack length, respectively, and K is the stress intensity factor (linear elastic). The factor η is taken equal to 2; E is the Young modulus and ν is the Poisson ration. More details on the J-integral formulation can be found in [12].

As it can be seen, in equation (1), the J-integral is incrementally evaluated using the actual crack length. It was shown in [10] that the crack extension can be estimated from the absorbed energy (area under the load-displacement test record). As a result, the crack extension can be determined using equation (3):

$$\Delta a_{(i)} \approx \Delta a_{final} \left(\frac{U_{(i)} - U_{init}}{U_{final} - U_{init}} \right)^2 \tag{2}$$

U_{init} is the energy required for crack growth onset. As it will be seen later, this threshold value corresponds to the onset of ductile crack initiation. Below this energy, no crack extension occurs, and therefore, $\Delta a=0$ if $U<U_{init}$.

Once J-values are calculated, the actual crack extension is re-calculated using equation (3):

$$\Delta a_{(i)} = \Delta a_{final} \left(\frac{J_{(i)} - J_{init}}{J_{final} - J_{init}} \right)^2 \tag{3}$$

As indicated in [9], this relation reflects simply the proportionality between the J–value with its derivative with respect to crack extension, namely the tearing resistance (*dJ/da*). Gioielli et al. [7] also assumed such a relation to derive the crack resistance from a Charpy impact test.

This procedure assumes that onset of crack initiation occurs at a load between the general yield (linear part) and the maximum load carrying capacity [9].

$$F_{init} = \frac{F_{gy} + F_{max}}{2} \tag{4}$$

This relation stems from the correlation between the shear fracture appearance and the characteristic loads of an instrumented Charpy impact test [13].

As a result, equation (1) for the J-integral and equation (3) for the crack extension allow to construct the crack resistance curve (R-curve). It can be shown that this R-curve follows a parabolic equation of the type:

$$J = J_{init} + J_t \sqrt{\Delta a} \tag{5}$$

where J_{init} is the J-value at the onset of ductile cracking and J_t measures the tearing resistance.

This procedure was extensively verified on a number of materials, geometries and experimental conditions [10-11]. Compared to other normalization procedures, such as the one proposed in the ASTM standard [12], this one is more closely based on the actual response of the material and applicable to specimens fully broken.

The same procedure can be applied to the notched rather than cracked geometry, namely the Charpy-V sample under impact loading. Figure 1 shows the load – time test traces of Charpy impact loaded samples of 20MnMoNi55 at 25 and 290°C and A533B at 290°C. The aim is to provide, using such a test record, an estimation of both quasi-static and dynamic (impact) crack resistance curves. However, a number of data manipulations are needed to be able to calculate the J-integral. To determine the area under the load–displacement curve, as specified by equation (1), the displacement, *s(t)*, should be calculated using the following equation:

$$s(t) = \int_{t_0}^{t} v(t)\, dt \tag{6}$$

where $v(t)$ is the actual velocity of the impact hammer given by:

$$v(t) = v_0 - \frac{1}{m}\int_{t_0}^{t} F(t)\, dt \tag{7}$$

v_0 and m are, respectively, the initial velocity and the mass of the impact hammer, $F(t)$ is the load at time t.
The absorbed energy, $U_{(i)}$, can then easily be calculated using equation (8):

$$U_{(i)} = \int_{0}^{s_{(i)}} F\, ds \tag{8}$$

For J-integral calculation, the same formulation as equation (1) is used except that the factor η is not constant (as in deeply notched samples) but changes with the crack configuration. Indeed, for a shallow crack, this factor was found to depend much on the crack length–to–width ratio and the following formulation, due to Sumpter [14] was adopted here:

$$\begin{cases} \eta = 0.32 + 12\left(\frac{a}{W}\right) - 19.5\left(\frac{a}{W}\right)^2 + 99.8\left(\frac{a}{W}\right)^3 & \frac{a}{W} < 0.282 \\ \eta = 2 & \frac{a}{W} \geq 0.282 \end{cases} \tag{9}$$

Note that the use of other formulations of the η-factor that are found in literature [15-16] do not affect the conclusions that will be drawn from the present work.

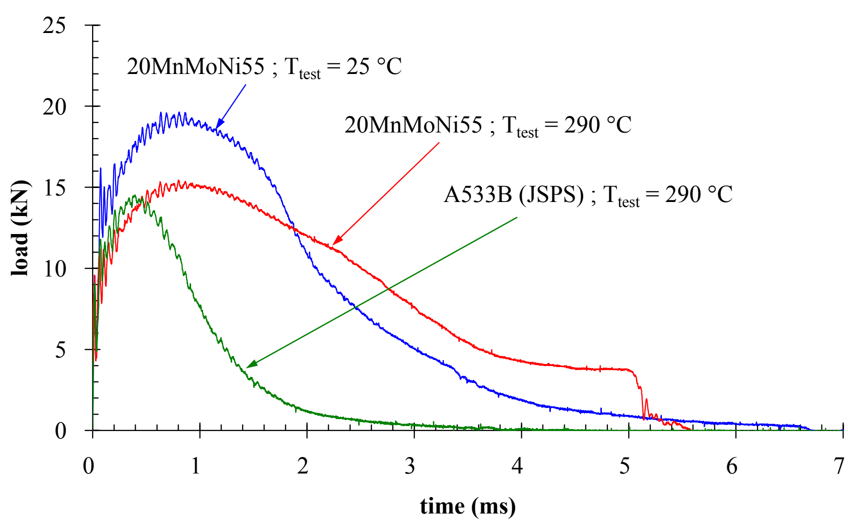

Figure 1. Load – time test records of Charpy impact tested specimens of 20MnMoNi55 and A533B steels.

Combining equation (1) and (9), the J-integral value can be evaluated at each data point. However, in the J-formulation, equation (1), the crack growth correction is not applicable for very large crack extensions. Indeed, above a certain crack extension, the J-integral value decreases with increasing crack extension. However, as it will be seen later, a good approximation can be obtained by maintaining the J-integral level at its maximum value in the region of decreasing J. It should be mentioned that in practice, fracture toughness tests are performed for limited crack extensions, generally not exceeding 10% of the ligament.

Materials and experimental conditions

Two reactor pressure vessel steels that were extensively investigated at SCK•CEN [13] were selected for the present investigation. These materials and the test temperature conditions provide a wide range of crack resistance behavior. An A533B plate provided by the Japan Society for the Promotion of Science (JSPS) which was artificially embrittled by S and P addition. As a result, the upper shelf energy is only 70 J and the DBTT is around +35°C. The second steel is the German 20MnMoNi55 steel, equivalent to an A508 forging with an upper shelf energy of about 180 J and a DBTT of -75°C; the DBTT being evaluated at 41J impact energy level. The chemical composition of the steels is given in Table 1.

Most of the tests performed here use the Charpy geometry. The choice of this geometry was motivated by three considerations. First, this geometry is used in the standardized notched bar impact test. Second, it can easily be tested statically as well as dynamically (impact). Finally, this geometry, when deeply precracked, was proven to lead to similar crack resistance behavior as large compact tension specimens [17]. Other considerations such as its small size and its availability in reactor pressure vessel surveillance programs could also be indicated. Basically, two configurations were used, the V-notch Charpy (standard Charpy geometry), and the precracked Charpy geometry with a crack depth–to–width ratio close to 0.5.

The standard Charpy specimen, referred to as CVN, is a 10×10×55 mm³ three-point bend specimen with a 45° V-notch of 2 mm depth. The samples that were fatigue precracked refer to as PCCv. For the quasi-static tests, the specimens were loaded in three-point bending on an electromechanically-driven Instron machine with a slow displacement rate (few tenths of mm/min). For the dynamic tests, the Charpy impact test machine was used, the available impact energy being adapted to produce the desired crack length. The J-rate corresponds to approximately 1 $kJ.m^{-2}.s^{-1}$ for the quasi-static tests and to 10^5 $kJ.m^{-2}.s^{-1}$ for the dynamic tests. Further details on the experimental procedure can be found in [9].

TABLE 1. Chemical composition

Material	C	Si	P	S	Cr	Mn	Ni	Cu	Mo
20MnMoNi55	0.19	0.20	0.007	0.008	0.12	1.29	0.80	0.11	0.53
A533B (JSPS)	0.24	0.41	0.028	0.023	0.08	1.52	0.43	0.19	0.49

As indicated above, the materials and test temperatures were selected such as three very distinct crack resistance curves could be obtained [9]. As a result, the 20MnMoNi55 forging was tested at 25 and 290°C while the A533B (JSPS) plate was tested at 290°C. This can be clearly seen on Figure 2 which compares the three crack resistance curves. The tensile properties are given in Table 2 for both static and dynamic loading rates.

TABLE 2. Tensile test results.

material	T_{test} (°C)	load rate	σ_y (MPa)	σ_u (MPa)	ε_u (%)	ε_t (%)	RA (%)
20MnMoNi55	25	static	450	595	10	23	75
20MnMoNi55	25	dynamic	522	666	11	24	75
20MnMoNi55	290	static	403	586	10	23	75
20MnMoNi55	290	dynamic	397	520	8	22	78
A533B (JSPS)	290	static	435	664	11	19	54
A533B (JSPS)	290	dynamic	433	574	9	19	63

To reduce the test matrix, the tests were selected such as to provide separate effects of each variable with the ultimate goal to provide the crack resistance from the CVN impact test. A number of experimental data were already given in [9]. Here, few additional data related to the specimen configuration effect, in particular the notch/crack acuity and depth will be given.

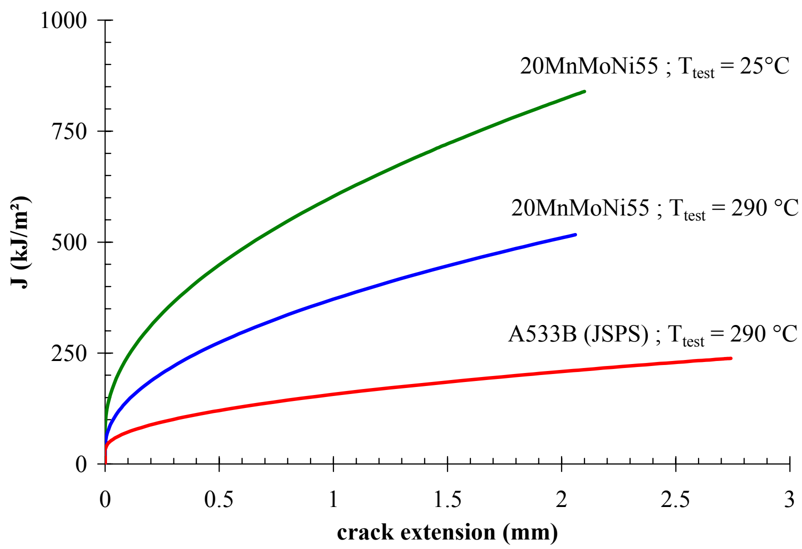

Figure 2. Comparative crack resistance behavior of 20MnMoNi55 and A533B (JSPS).

The main objective being the determination of the crack resistance (quasi-static and dynamic) from the standard Charpy impact test, it will be necessary to evaluate both the notch versus crack effect and the shallow versus deep crack configuration. The tests will be appropriately selected to evaluate both effects.

The crack resistance curves at both static and dynamic loading rates were taken from [9]. The loading rate effect is assumed to be similar to what was found in [9], namely the proportionality constant $\alpha_{loading\ rate}$ and the square of the yield strength ratio, $\left(\frac{\sigma_y^{dynamic}}{\sigma_y^{static}}\right)^2$. As it will also be seen here, the experimental data obtained here support such an assumption. Focus of the experimental work presented here is put on the effect of notch acuity and notch/crack depth. The following tests were performed (see Figure 3):

- CVN low blow tests at static loading: the standard Charpy specimens were loaded in three-point slow bending up to various crack extensions, the absorbed energies varying between about 4 to 110 J.
- PCCv low blow tests at impact loading: the precracked Charpy specimens with a/ a/W≈0.5 were impact loaded with an available energy between about 5 to 40 J.

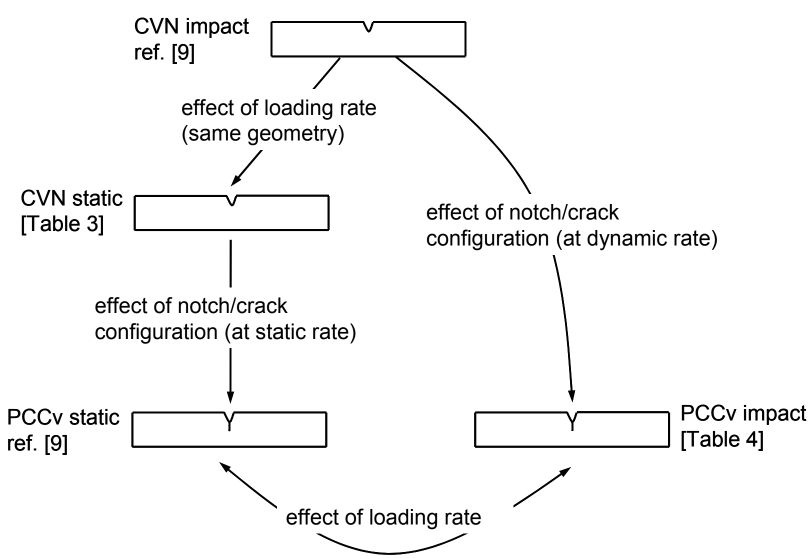

Figure 3. Schematic diagram showing the combined effects of specimen configuration and loading rate.

Results

The results of the various tests are given in Tables 3 to 4. The data of Table 3 can be used to relate the shallow notch (a/W=0.2) of a Charpy specimen to the deep crack (a/W=0.5) of a three-point bend specimen (precracked Charpy). The J-calculation according to the procedure described above lead to the results shown in Figure 4. This Figure demonstrates the possibility to use a fully broken single specimen to describe the crack resistance based on a V-notch geometry.

TABLE 3. Slow bend test results on Charpy V-notched samples.

material	T	W	B	a_0	U	Δa	J_0
20MnMoNi55	25	10.00	10.00	2	13.3	0.07	289
20MnMoNi55	25	10.00	10.00	2	31.9	0.27	694
20MnMoNi55	25	9.99	10.00	2	48.4	0.68	1045
20MnMoNi55	25	9.99	9.99	2	69.0	1.38	1456
20MnMoNi55	25	10.00	9.99	2	88.8	2.20	1806
20MnMoNi55	25	9.96	9.91	2	107.0	4.77	1852
20MnMoNi55	290	10.00	10.01	2	8.7	0.03	190
20MnMoNi55	290	9.99	10.00	2	20.7	0.30	451
20MnMoNi55	290	10.00	10.00	2	36.0	0.79	837
20MnMoNi55	290	9.99	10.00	2	42.2	1.21	896
20MnMoNi55	290	10.00	10.00	2	54.2	1.96	1114
20MnMoNi55	290	10.00	9.99	2	73.4	3.04	1430
20MnMoNi55	290	9.97	9.94	2	79.6	5.44	1309
A533B (JSPS)	290	10.00	10.01	2	4.2	0.01	91
A533B (JSPS)	290	9.98	10.01	2	8.9	0.04	194
A533B (JSPS)	290	10.00	10.01	2	11.3	0.21	245
A533B (JSPS)	290	10.01	10.01	2	15.0	0.30	326
A533B (JSPS)	290	10.01	10.02	2	14.4	0.35	313
A533B (JSPS)	290	10.00	10.01	2	18.1	0.98	385
A533B (JSPS)	290	10.00	10.01	2	20.0	1.41	349
A533B (JSPS)	290	10.00	10.00	2	21.7	1.63	447
A533B (JSPS)	290	9.98	9.94	2	27.5	2.43	544
A533B (JSPS)	290	9.98	9.94	2	30.7	4.12	547

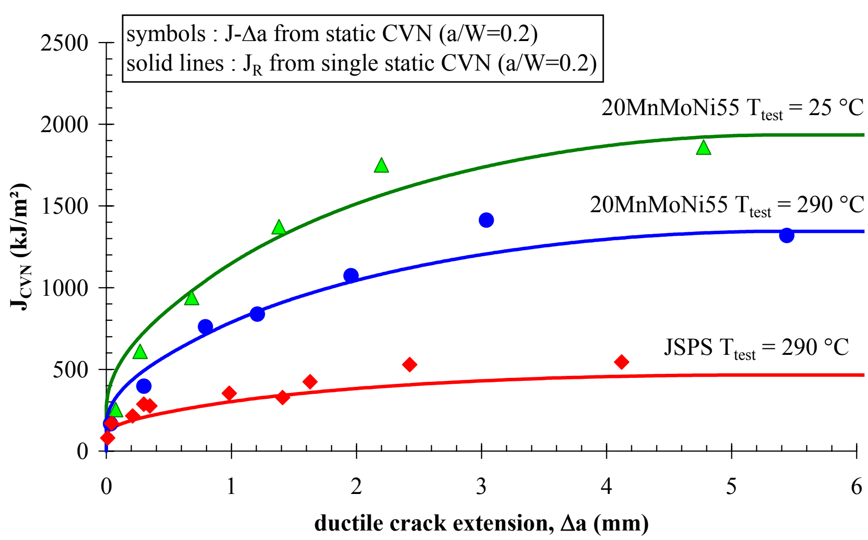

Figure 4. J-R curves from static CVN Charpy V-notched specimens. Apparent high crack resistance due to notch configuration (twice higher toughness than in Figure 2).

In [9], the dynamic crack resistance curves were obtained using a single precracked specimen. Most of the data for which the procedure was validated were quasi-static tests. Here, we performed a number of tests (multiple specimen method) to demonstrate the applicability of the procedure to dynamic loading rate. The results are summarized in Table 4 and Figure 5 shows the good agreement between the various samples..

TABLE 4. Impact test results on precracked Charpy samples.

material	**T**	**W**	**B**	**a_0**	**U**	**Δa**	**J_0**	**remark**
20MnMoNi55	25	9.93	9.92	5.17	9.1	0.17	393	
20MnMoNi55	25	9.95	9.91	5.11	13.9	0.37	567	
20MnMoNi55	25	9.94	9.90	5.25	18.6	0.54	774	
20MnMoNi55	25	9.97	9.96	5.20	23.4	1.05	900	
20MnMoNi55	25	9.93	9.90	5.17	28.1	1.30	1056	
20MnMoNi55	25	9.95	9.93	5.30	31.4	1.61	1146	
20MnMoNi55	25	9.97	9.93	5.04	34.3	1.79	1174	
20MnMoNi55	25	9.92	9.94	5.44	39.0	2.45	1292	from [9]
20MnMoNi55	290	9.94	9.87	5.04	9.5	0.26	381	
20MnMoNi55	290	9.96	9.93	5.28	14.5	0.54	585	
20MnMoNi55	290	9.94	9.91	5.02	19.2	0.60	740	
20MnMoNi55	290	9.95	9.91	5.26	24.0	0.87	936	
20MnMoNi55	290	9.96	9.94	5.16	28.9	1.24	1068	
20MnMoNi55	290	9.96	9.90	4.91	33.5	1.61	1142	
20MnMoNi55	290	9.93	9.89	5.13	36.8	2.41	1176	from [9]
A533B (JSPS)	290	10	10	5.62	6.2	0.35	259	
A533B (JSPS)	290	10	10	4.93	8.0	0.59	286	
A533B (JSPS)	290	10	10	5.38	10.2	1.02	296	
A533B (JSPS)	290	10	9.95	5.43	12.1	1.55	430	
A533B (JSPS)	290	9.94	9.90	5.15	14.4	2.04	492	
A533B (JSPS)	290	9.96	9.95	5.29	16.8	2.21	562	from [9]
A533B (JSPS)	290	9.92	9.84	5.18	18.3	2.79	560	
A533B (JSPS)	290	10.02	9.95	5.28	21.3	4.75	512	

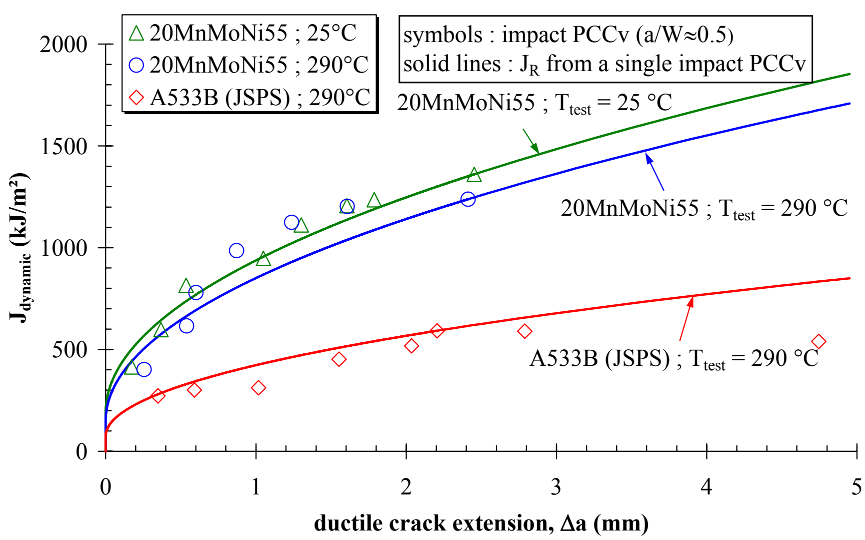

Figure 5. Dynamic crack resistance. The solid lines based on a single precracked specimen.

Analysis of the Results

In the preceding section, it was shown that the procedure for crack resistance determination is adequate for both notched samples and at dynamic loading rates. It was also shown in [9] that the static J_R-curve can be derived from the dynamic one using the following equation:

$$J_R^{static} = \alpha_{loading\ rate} \times \left(\frac{\sigma_y^{dynamic}}{\sigma_y^{static}} \right)^2 \times J_R^{dynamic} \tag{10}$$

where the constant $\alpha_{loading\ rate}$ approximately equal to 0.46. This equation, denoting the effect of loading rate on the loss of crack tip constraint, was obtained with deep cracked samples. For shallow cracks, it is known that an apparent crack resistance elevation is observed as a result of loss of constraint [18]. We have also seen in [9] that a good correlation seems to exist between the V-notched geometry and the cracked geometry. So, we can adopt the same strategy as for the loading rate effect by introducing a factor that accounts for the crack configuration effect (deep versus shallow crack). Similarly to equation (9), one can write:

$$J_R^{deep\ crack} = \alpha_{shallow>deep} \times J_R^{shallow\ crack} \tag{11}$$

where $\alpha_{shallow>deep}$ accounts for the loss of constraint introduced by the shallow crack.

Because of the crack blunting phenomenon that occurs before fracture initiation, it is assumed that the notch acuity (notch versus crack) will not have a significant influence on the crack resistance behavior. As it will be seen later, this assumption is reasonable. Indeed, consistent results are obtained based on this assumption. Experimental validation using shallow precracked specimens is in progress for a complete justification.

Combining equations (9) and (10), one obtains the relation allowing determination of the static crack resistance using the Charpy impact test::

$$J_R^{static} = \alpha_{loading\ rate} \times \alpha_{shallow>deep} \times \left(\frac{\sigma_y^{dynamic}}{\sigma_y^{static}} \right)^2 \times J_R^{CVN\ impact} \tag{12}$$

To obtain the dynamic crack resistance, equation (11) reduces to:

$$J_R^{dynamic} = \alpha_{shallow>deep} \times J_R^{CVN\ impact} \tag{13}$$

So, equations (11) and (12) can be used to correlate the crack resistance obtained from the Charpy impact test with the static and dynamic crack resistance curves. The crack resistance curve from a Charpy specimen can easily be obtained from the instrumented Charpy impact test. We can determine the factor $\alpha_{shallow>deep}$ that rationalize the results. A unique factor, rationalizing all experimental result, was found, $\alpha_{shallow>deep}$ = 0.55. At static loading rate, Figure 6 shows the good agreement between the Charpy V- notch sample and the precracked geometry. As it can be seen, ignoring the effect of notch acuity and considering only the specimen configuration, namely shallow notch versus deep crack, both geometries lead to very similar results. The same static Charpy V-notched results shown in Figure 6 are compared in Figure 7 to crack resistance curve obtained using a single Charpy impact test. The agreement is very good. For the dynamic crack resistance, Figure 8 shows the precracked Charpy specimens are also in very good agreement with the crack resistance derived from the Charpy impact test, the latter being obtained using equation (12). Finally, Figure 9, summarizing all available data, shows an excellent agreement between the various geometries. This Figure clearly supports the capability determining both the static and dynamic crack resistance curves from a single instrumented Charpy impact test.

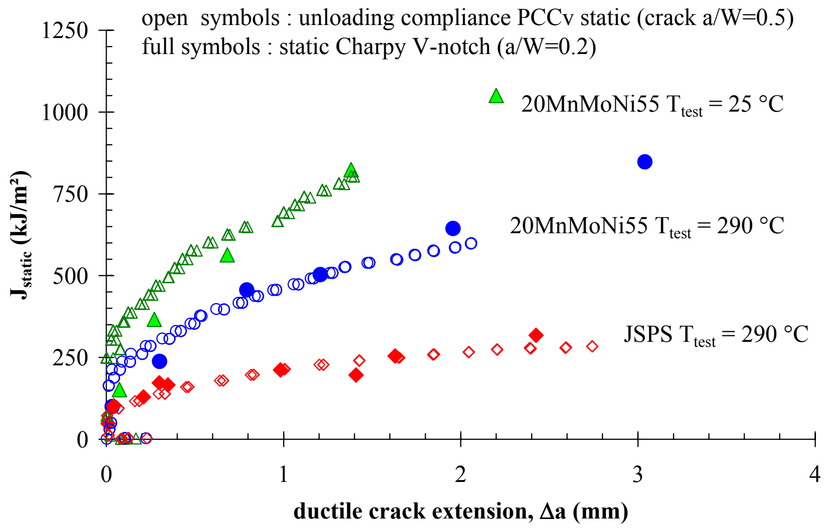

Figure 6. Static Charpy V-notch versus precracked Charpy (obtained using the unloading compliance method). Crack configuration effect is accounted for through $\alpha_{deep>shallow}$.

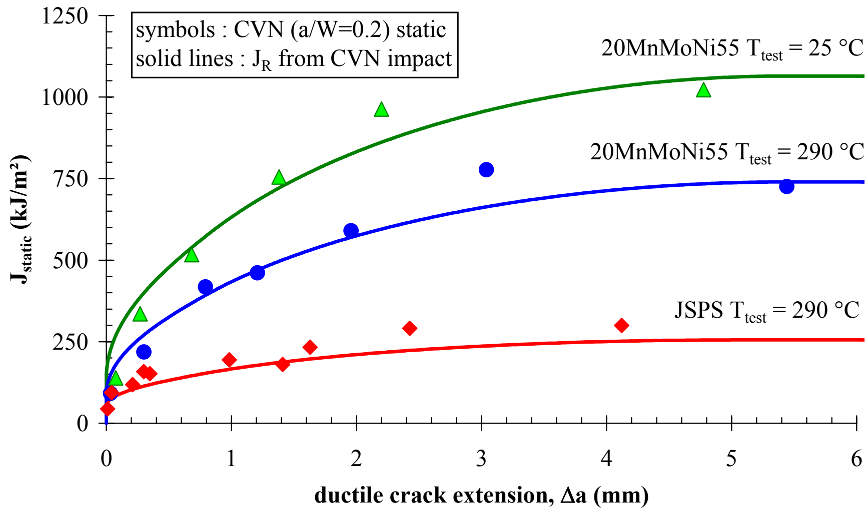

Figure 7. Crack resistance curve as derived from the static Charpy V-notch geometry, accounting for the crack configuration effect through $\alpha_{deep>shallow}$.

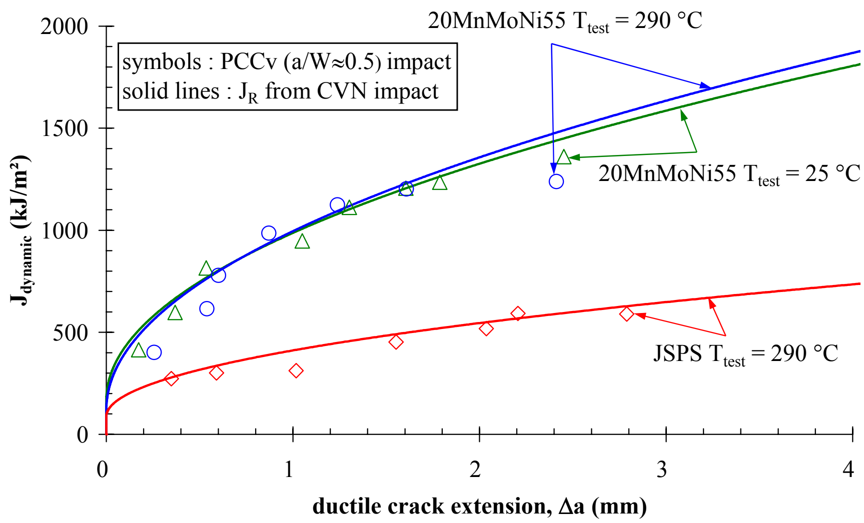

Figure 8. Dynamic crack resistance behavior of 20MnMoNi55 and A533B (JSPS). Solid lines are obtained from a single Charpy impact test while symbols designate the multiple PCCv specimen method.

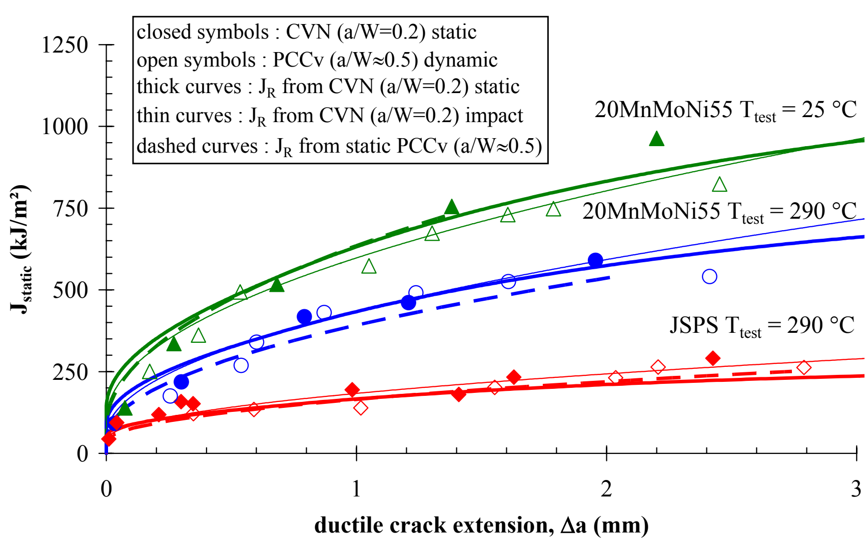

Figure 9. Summary of the various crack resistance curves of 20MnMoNi55 and A533B (JSPS).

Discussion

A number of fracture toughness–Charpy upper shelf energy correlations were proposed in literature. A review of the different correlations can be found in [4,8]. As already indicated in [9], the main drawback of such correlations is their inability to account for the decrease of static fracture toughness with increasing upper shelf temperature. Indeed, in the upper shelf regime, both dynamic fracture toughness and Charpy impact energy remain little or unaffected by increasing test temperature, By contrast, at quasi-static loading rates, both fracture toughness and Charpy energy decrease with increasing temperature. Nevertheless, it is interesting to compare our procedure with those proposed in literature, in particular Schindler [6], Gioielli et al. [7] and Wallin [8] for which a full J_R curve can be drawn. To illustrate these comparisons, two J-parameters were selected, $J_{0.2}$ and J_2 corresponding to 0.2 mm and 2 mm crack extension, respectively. The former corresponds to crack initiation and the second roughly to the tearing capacity. These parameters were determined using fracture mechanics tests, namely the deeply precracked Charpy specimens. These reference values are then compared to the values determined from a single Charpy impact test. As it can be seen from Figure 10 for dynamic loading and Figure 11 for quasi-static loading, the procedure presented in this paper is clearly leads to a better agreement with the values determined with fracture toughness specimens. Note that the uncertainty bounds shown on Figure 11 are equal to those given in [7] and [8], and they correspond to about 30%-relative uncertainty. It is important to emphasize that these three correlations are based only on the total absorbed energy to fully fracture an 8 mm ligament. By contrast, our procedure is based on the full load–displacement curve.

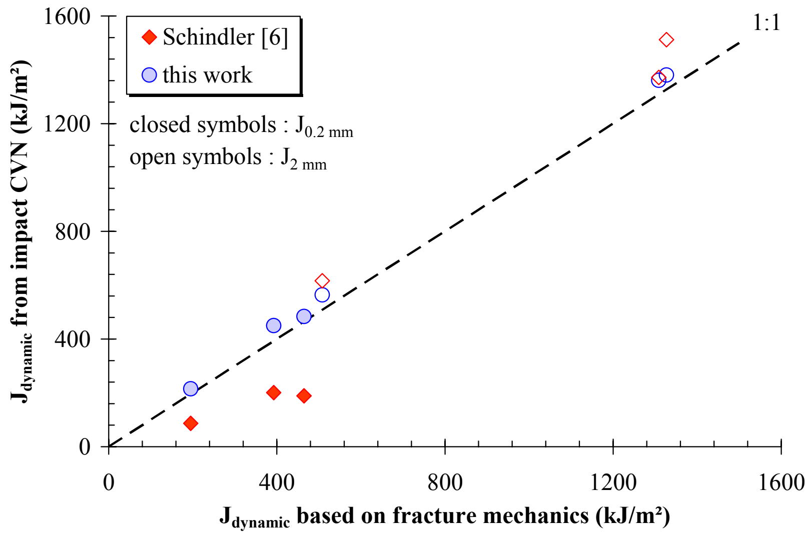

Figure 10. Comparison with other correlations determining dynamic crack resistance from the Charpy impact test.

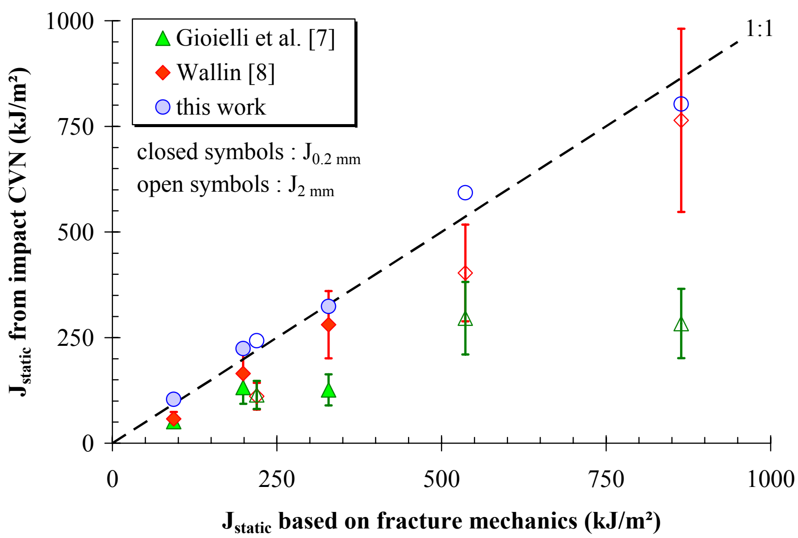

Figure 11. Comparison with other correlations determining static crack resistance from the Charpy impact test.

There are limitations of the procedure presented here, in particular the application of equation (13). These are mainly related to the constants accounting for notch/crack configuration and loading rate. These constants were empirically established on the basis of experimental results. Therefore, application to other material and experimental conditions will probably need re-evaluation of thse constants. Because these constants were introduced to account for the loss of constraint, it will be very much interesting to relate these them directly to the actual loss of constraint calculations using finite element computations. A number of such calculations were already performed to evaluate the loss of constraint induced by crack configuration and loading rate, for example [19-20]. Analytical expressions can then be established on the basis of finite element of the form:

$$\alpha_{loss\ of\ constraint} = \alpha_{shallow>deep}\ \alpha_{loading\ rate} = f\left(\frac{\sigma_y}{E}, n, a/W, \dot{J}\right) \quad (14)$$

where all important parameters related to material, crack configuration and loading rate are taken into account. Equation (14) can be fitted to the finite element results. For the specific case of the material, specimen configuration and loading rate conditions investigated here, this function shoud lead to a loss of constraint constant of about 0.25.

Conclusions

This study has demonstrated the possibility to accurately determine the crack resistance behavior from the instrumented Charpy impact test. The procedure is solely based on the instrumented Charpy impact test record. Both dynamic and static crack resistance can be derived with a high accuracy. Test temperature and loading rate effects are correctly accounted for by the constants introduced to take the induced loss of constraint into account. These constants were experimentally determined for the material, specimen configuration and loading rate conditions investigated here. But to increase the range of application, a better account of these effects would be possible by performing appropriate finite element calculations that can be analytically expressed as a function of crack depth–to–width ratio and loss of triaxiality.

Acknowledgments

The authors gratefully acknowledge the technical support of R. Mertens, A. Pellettieri and L. Van Houdt. The steels, 20MnMoNi55 and A533B (JSPS) were kindly provided by J. Heerens (GKSS) and K. Onizawa (JAERI), respectively.

References

1. Rolfe S.T. and Barsom, J.M., Fracture and Fatigue Control in Structure – Application of Fracture Mechanics, Prentice-Hall, Inc., Englewood Cliffs, New Jersey, 1977.
2. Rolfe, S.T. and Novak, S.R., Slow-bend K_{Ic} testing of medium-strength high-toughness steels, Review of Development in Plane Strain Fracture Toughness Testing, ASTM STP 463, American Society for Testing and Materials, 124-159, 1970.
3. Barsom, J.M. and Rolfe, S.T., Correlation between K_{Ic} and Charpy V-notch test results in the transition temperature range, Impact Testing of Metals, ASTM STP 466, American Society for Testing and Materials, 281-302, 1970.
4. Pisarski, H.G., A review of correlations relating Charpy energy to K_{Ic}, The Welding Institute Research Bulletin, 362-367, December 1978.
5. Nageswara Rao B. and Acharya, A.R., A computer study on evaluation of fracture toughness from Charpy V-notch impact energy and reduction of area, Engineering Fracture Mechanics, Vol. 41, No. 1, 85-90, 1992.
6. Schindler, H.J., Estimation of the dynamic J-R curve from a single impact bending specimen, Proceedings of the 11th European Conference on Fracture, ECF-11, Mechanisms and Mechanics of Damage and Failure, J. Petit, Ed., Vol. II, 2007-2012, 1996.
7. Gioielli, P.C., Landes, J.D., Paris, J.D., Tada, H. and Loushin, L., Method for predicting J-R curves from Charpy impact energy, Fatigue and Fracture Mechanics: 30th Volume, ASTM STP 1360, P.C. Paris and K.L. Jerina, Eds., American Society for Testing and Materials, 61-68, 2000.
8. Wallin, K., Low cost J-R curve estimation based on CVN upper shelf energy, Fatigue and Fracture of Engineering Materials and Structures, 24, 537-549, 2001.
9. Chaouadi, R. and Puzzolante, J.L., Loading rate effect on ductile fracture, submitted to ECF-16, (in preparation).
10. Chaouadi, R., An energy-based crack extension formulation for crack resistance characterization of ductile materials, Journal of Testing and Evaluation, Vol. 32, No. 6, 469-475, 2004.
11. Chaouadi, R., "Crack resistance determination from the load – displacement test record", SCK•CEN Report, R-3712, March 2003.
12. ASTM, E 1820-01, Standard Test Method for Measurement of Fracture Toughness, Annual Book of ASTM Standards, Section III, Metals Test Methods and Analytical Procedures, Volume 03.01, American Society for Testing and Materials, 2002.
13. Chaouadi, R. and Fabry, A., On the utilization of the instrumented Charpy impact test for characterizing the flow and fracture behavior of reactor pressure vessel steels, From Charpy to Present Impact Testing, edited by D. François and A. Pineau, Elsevier, 103-117, 2002.
14. Sumpter, J.D.G., J_c–determination for shallow notch welded bend specimens, Fatigue and Fracture of Engineering Materials and Structures, Vol. 10, n° 6, 479-493, 1987.
15. Nevalainen, M. and Wallin, K., The effect of crack depth and absolute thickness on fracture toughness of 3PB specimnes, Proceedings of the 10th European Conference on Fracture, ECF-10, Structural Integrity: Experiments, Models and Applications, K.H. Schwalbe and C. Berger, Eds., Vol. II, 997-1006, 1994.
16. Sreenivasan, P.R. and Mannan, S.L., Plastic η-factor for three-point bend specimens: Analysis of instrumented Charpy impact test results for AISI 308 weld and AISI 316 stainless steels, International Journal of Fracture, 101, 215-228, 2000.

17. Chaouadi, R., Analysis o fracture toughness behavior of 22NiMoCr37 steel in the transition regime (SM&T round robin), SCK•CEN Report, BLG-799, December, 1998.
18. L. Tosal, G. Rodriguez, F.J. Belzunce and C. Betegon, The influence of specimen size on the fracture behavior of a structural steel at different temperatures, Journal of Testing and Evaluation, Vol. 28, No. 4, 2000, pp. 276-281.
19. Anderson, T.L. and Dodds, R.H. Jr., Specimen size requirements for fracture toughness testing in the transition region, Journal of Testing and Evaluation, Vol. 19, No. 2, 123-134, 1991.
20. Koppenhoefer, K.C. and Dodds, R.H., Ductile crack growth in pre-cracked CVN specimens: numerical studies, Nuclear Engineering and Design, 180, 221-241, 1998.